Geophysical Research Letters

RESEARCH LETTER
10.1029/2023GL105304

A Non-Dimensional Index for Characterizing the Transition of Turbulence Regimes in Stable Atmospheric Boundary Layers

Xin Shao[1], Ning Zhang[1,2], Dan Li[3], and Jianning Sun[1,4]

[1]School of Atmospheric Sciences, Nanjing University, Nanjing, China, [2]Key Laboratory of Urban Meteorology, China Meteorological Administration, Beijing, China, [3]Department of Earth and Environment, Boston University, Boston, MA, USA, [4]Joint International Research Laboratory of Atmospheric and Earth System Sciences, Nanjing University, Nanjing, China

Key Points:

- A critical horizontal Froude number (≈0.28) is proposed to characterize the transition from moderate to weak turbulence regimes
- The critical horizontal Froude number corresponds to the development of pancake vortices
- Previously used height- and site-dependent mean wind speed thresholds can be recovered from the critical horizontal Froude number

Supporting Information:

Supporting Information may be found in the online version of this article.

Correspondence to:

N. Zhang,
ningzhang@nju.edu.cn

Citation:

Shao, X., Zhang, N., Li, D., & Sun, J. (2023). A non-dimensional index for characterizing the transition of turbulence regimes in stable atmospheric boundary layers. *Geophysical Research Letters*, *50*, e2023GL105304. https://doi.org/10.1029/2023GL105304

Received 2 JUL 2023
Accepted 30 AUG 2023

Abstract The transition from moderate to weak turbulence regimes remains a grand challenge for stable boundary layer parameterizations in weather and climate models. In this study, a critical horizontal Froude number (≈0.28) is proposed to characterize such a transition, which corresponds to the development of quasi two-dimensional pancake vortices. Traditionally defined stability parameters corresponding to the critical horizontal Froude number are estimated and are consistent with values in the literature. The critical horizontal Froude number can recover previously used height- and site-dependent mean wind speed thresholds. These findings offer a way to constrain the validity range of Monin-Obukhov similarity theory in numerical models for weather and pollutants dispersion.

Plain Language Summary The transition from moderate to weak turbulence regimes in stable atmospheric boundary layers presents a grand challenge for numerical models. Our results show that such a transition occurs when the horizontal Froude number is equal to a critical value of about 0.28, which is physically connected to the development of quasi two-dimensional pancake vortices. These findings can help improve turbulence parameterizations in numerical models for weather and pollutants dispersion.

1. Introduction

Monin-Obukhov similarity theory (MOST, Monin & Obukhov, 1954) is regarded as the starting point for modern micrometeorology (Foken, 2006; Nieuwstadt, 1984) and has been a cornerstone of surface-layer turbulence parametrization in weather and climate models (e.g., Hong et al., 2006; Nakanishi & Niino, 2006; Pleim, 2007). In numerical models, bulk formulations equivalent to MOST, which relate turbulent fluxes to mean flow properties, are widely used. For example, turbulent momentum flux is often expressed as $u_*^2 = C_d U^2$, where u_* is the friction velocity, C_d is the drag coefficient, and U is the mean wind speed. The validity range of MOST or bulk formulations in stable atmospheric boundary layers remains a long-standing issue (Holtslag et al., 2013; Mahrt, 2014). Much effort has been devoted to investigating the breakdown of MOST (e.g., Grachev et al., 2013) and its association with flow laminarization. However, observed data indicate that flow laminarization under strong stratification is questionable (Galperin et al., 2007). Instead, the turbulent flow seems to transition into a weak regime where a finite amount of mixing remains (Mahrt, 2014).

A common way to distinguish different regimes of stable atmospheric boundary layers is through the variation of u_* with U (Sun et al., 2012; Van de Wiel et al., 2012). In this method, two regimes are often identified: a weak turbulence regime where the mean wind speed is less than a height-dependent threshold (U_s) and a moderate turbulence regime where the mean wind speed exceeds U_s. The friction velocity u_* increases weakly with the mean wind speed U in the weak turbulence regime, but increases strongly with the mean wind speed U in the moderate turbulence regime. Sun et al. (2016) named such a transition as HOckey-Stick Transition (HOST). Similar findings have been reported in follow-up studies using observations and numerical models (Acevedo et al., 2019; Chechin, 2021; Maroneze et al., 2019). It is suggested that the transition is due to changes in the coupling states of the surface layer (Acevedo et al., 2016; Sun et al., 2016, 2020), which are modulated by coherent eddies across the layers. In coupled surface layers, these coherent eddies are attached to the ground and are vertically synchronized (coupled), which provide the foundation for the bulk formulations and MOST. Because of these coherent eddies, the surface layer simultaneously experiences enhanced turbulent mixing of momentum and heat (Cuxart et al., 2002; Lan et al., 2018, 2019). In decoupled surface layers, turbulent eddies are

depressed and detached from the surface, leading to suppressed vertical mixing and the breakdown of bulk formulations and MOST. Knowledge on the transition between the two turbulence regimes is crucial for constraining the application range of MOST and for further improving turbulence parameterizations in stable boundary layers (Mahrt, 2014; Sandu et al., 2013).

Researchers have not agreed upon which index works best to characterize the transition between the two turbulence regimes in stable atmospheric boundary layers. The mean wind speed threshold (U_s), as a dimensional quantity, cannot be expected to be universal (Mahrt et al., 2015; Van de Wiel et al., 2012). The dual characteristics of heat flux and the stability parameter corresponding to the maximum heat flux (in terms of magnitude) (Lapworth & Osborne, 2020; Mahrt et al., 1998; Malhi, 1995), albeit widely studied and recognized, have been found to fail to separate turbulence regimes as the maximum heat flux tends to occur in the weakly stable regime (Acevedo et al., 2019). The Richardson numbers (including the gradient Richardson number and the flux Richardson number) have been extensively studied, motivated by the seminar work by Miles and Howard (Howard, 1961; Miles, 1961; Miles & Howard, 1964), yet the exact meaning of critical (or sometimes maximum) Richardson numbers remains to be clarified (Bou-Zeid et al., 2018; Galperin et al., 2007; Katul et al., 2014; Li et al., 2015). Other work proposed non-dimensional indices to characterize horizontal meandering (Mortarini et al., 2019) and vertical coupling (Peltola et al., 2021), but the exact transition thresholds for these indices remain empirically determined. This study aims to bridge this research gap by proposing a new non-dimensional index for characterizing the transition between moderate and weak turbulence regimes and determining the transition threshold value theoretically. In the following, the data set and methodology are elaborated in Section 2; a theoretical model is introduced in Section 3; interpretations of results are presented in Section 4; conclusions and discussion can be found in Section 5.

2. Data and Methods

2.1. Data Set

The data from the Cooperative Atmosphere-Surface Exchange Study in October 1999 (CASES-99) field experiment are used (Poulos et al., 2002). The CASES-99 data set contains ultrasonic turbulence measurement on a 60-m tower in southeast Kansas (located at 37.649°N, 96.736°W) during the month of October 1999. The tower site was surrounded by the relatively flat terrain. Sonic anemometers were installed at 1.5, 5, 10, 20, 30, 40, 50, and 55 m. Since the lowest sonic anemometer was moved on 20 October, the measurements at 1.5 m are not used in this study. Data are split into 15-min segments.

2.2. Data Processing

The coordinate system is defined that x, y, and z-coordinates represent the streamwise direction, the spanwise direction, and the vertical direction, respectively, and the corresponding velocity components are u, v, and w. Due to this rotation, the spanwise mean wind speed and the spanwise momentum flux become sufficiently small and are neglected. The mean wind speed is then defined as $U = \overline{u}$, where the overbar represents the time average. Turbulent momentum fluxes and heat fluxes are computed as $-\overline{u'w'}$ and $\overline{w'\theta'}$ with the prime indicating the turbulent fluctuations from the time averages, and the friction velocity is calculated as $u_* = \sqrt{-\overline{u'w'}}$. Brunt-Väisälä frequency is defined as $=\left(\frac{g}{\theta}\frac{\partial\overline{\theta}}{\partial z}\right)^{\frac{1}{2}}$, where θ denotes the potential temperature, g is gravity acceleration, and z denotes the distance to the ground. The mean wind speed gradient $S = \frac{\partial U}{\partial z}$ and the mean potential temperature gradient $\frac{\partial\overline{\theta}}{\partial z}$ are obtained by fitting third-order polynomial functions to the mean wind speed and mean potential temperature profiles and then taking the derivative of the fitted functions. Using the above definitions, the Obukhov length is computed as $L = -\theta u_*^3 / \left(\kappa g \overline{w'\theta'}\right)$, where κ is Karman constant. The stability parameter z/L can be used to measure the atmospheric stability. Another widely used stability parameter, the gradient Richardson number, is computed as $Ri_g = \frac{N^2}{S^2}$. The dissipation rate for turbulence kinetic energy ϵ is obtained from its relation with the second-order structure function $S_2(r)$ as $S_2(r) = 2.13\epsilon^{\frac{2}{3}} r^{\frac{2}{3}}$ (Kolmogorov, 1941), where $S_2(r) = \overline{\left(u\left(t + \frac{r}{U}\right) - u(t)\right)^2}$ with t the time and r the separation scale following Taylor's frozen eddy hypothesis.

The streamwise and vertical turbulence integral length scales are obtained by fitting exponential functions to the autocorrelation as (Salesky et al., 2013):

$$R_{uu}(\Delta x, 0) = \exp\left(-\frac{|\Delta x|}{L_h}\right), \tag{1}$$

$$R_{uw}(0, \Delta z) = \exp\left(-\frac{|\Delta z|}{L_v}\right), \tag{2}$$

where $R_{uu}(\Delta x,0)$ and $R_{ww}(0,\Delta z)$ denote the streamwise and vertical autocorrelation which are calculated as $R_{\alpha\alpha}(\Delta x, \Delta z) = \frac{\overline{\alpha'(x+\Delta x,z+\Delta z)\alpha'(x,z)}}{\sqrt{\overline{\alpha'(x+\Delta x,z+\Delta z)^2}}\sqrt{\overline{\alpha'(x,z)^2}}}$ with α denoting u and w, Δx, and Δz denote the streamwise and vertical spatial lags, and L_h and L_v denote the streamwise and vertical integral length scales (Li, 2020; Salesky et al., 2013). An example of deriving L_v through fitting is given in Figure S1 in Supporting Information S1. It can be seen that the fitting method is reasonable for all reference heights except the lowest one (5 m), and thus the calculated L_v at 5 m is discarded.

The horizontal Froude number is defined as $F_h = \frac{\sigma_u}{NL_h}$, where σ_u is the standard deviation of streamwise velocity. The buoyancy length scale is defined as $L_b = \frac{\sigma_u}{N}$, which represents the vertical displacement of a fluid parcel if all its kinetic energy were converted to potential energy (Billant & Chomaz, 2000b). In this sense, the horizontal Froude number can be regarded as the ratio of the buoyancy length scale to the streamwise turbulence integral length scale. Similarly, the vertical Froude number can be defined as $F_v = \frac{\sigma_u}{NL_v}$, which represents the ratio of the buoyancy length scale to the vertical turbulence integral length scale. Note that the vertical Froude number is still defined with σ_u, not the standard deviation of vertical velocity (σ_w). This is a major difference between our work and the study by Peltola et al. (2021). We choose σ_u as again $\frac{\sigma_u}{N}$ represents the vertical displacement of a fluid parcel if all its kinetic energy were converted to potential energy (Billant & Chomaz, 2000b; Riley & Lindborg, 2008) while $\frac{\sigma_w}{N}$ only represents the vertical displacement of a fluid parcel within the buoyancy time scale.

3. Theory

Our starting point of characterizing the transition is to assume that the turbulence regime transition concurs with the development of quasi two-dimensional pancake vortices, which provides a constraint on the vertical length scale of turbulence. Vortex instability (Herring & Métais, 1989) in stably stratified fluid has been investigated by setting long vertical columnar vortex pair experimentally and numerically (Billant & Chomaz, 2000a, 2000b, 2000c; Leweke & Williamson, 1998). For weak stratification, the elliptic instability prevails by the gradual bending of each vortex core in the opposite direction to the vortex periphery. As stratification becomes stronger, the zigzag instability plays an increasingly important role. The vortex pair twists with almost no change of the dipole's cross-sectional structure and is ultimately sliced into thin horizontal layers of independent pancake dipoles. Under such conditions, turbulence behaves as quasi two-dimensional pancake vortices. However, we note that the dynamics of these pancake vortices remain closer to three-dimensional turbulence rather than exact two-dimensional turbulence (Sozza et al., 2015).

Since the shape of pancake vortices is buoyancy driven, the horizontal Froude number, as a stability parameter for assessing buoyancy effects, is often used to describe the development and evolution of pancake vortices with stratification (Mater & Venayagamoorthy, 2014a, 2014b). Further analysis showed that the typical thickness of pancake layers scales with the buoyancy scale (Billant & Chomaz, 2001; Lindborg, 2006; Riley & Lindborg, 2008). Thus, we expect F_v approaches unity at the transition (i.e., $F_{vc} = 1$ where the subscript c indicates critical) with the development of pancake vortices. However, it is much difficult to compute F_v as it requires ultrasonic measurements at multiple heights and data fitting across heights (Figure S1 in Supporting Information S1). In contrast, the horizontal Froude number F_h only requires ultrasonic measurements at a single height. Therefore, for practical purposes, it is better to formulate the transition in terms of F_h instead of F_v.

Building on this thinking, our model starts in the weak stratification and then identify the transition (i.e., a critical F_h value) by introducing the constraint of $F_{vc} = 1$ at the transition. By starting from weak stratification, many assumptions in our theoretical model should still be applicable. Essentially, we aim to derive a relation between

F_h and F_v, which requires to derive a relation between L_h and L_v. This is accomplished by using a simplified spectral model introduced below.

While the Kolmogorov −5/3 power law scaling for isotropic turbulence ends at the Ozmidov scale that indicates the largest scale of isotropic turbulence (Li et al., 2016), Lindborg (2006) reported that a new −5/3 power law scaling holds for anisotropic turbulence bounded in pancake layers. The new −5/3 power law scaling in this so-called buoyancy subrange has received some support from atmospheric surface layer studies (Cheng et al., 2020), but the mechanism for the new −5/3 power law scaling differs from that in isotropic turbulence. Energy is first transferred directly from the large scales to the Ozmidov scale by the zigzag instability and Kelvin–Helmholtz instability, and then transferred to the Kolmogorov scale by the traditional energy cascade process described by the Kolmogorov theory (Deloncle et al., 2008). Given these results, we assume the −5/3 power law scaling extends from the integral length scale to the inertial subrange of isotropic turbulence. To facilitate analytical treatment, we further ignore the spectral drop in the dissipation range. This is justified given that the dissipation range contributes little to the total energy (variance). At the low frequency end, we assume that the spectra flatten once the scale becomes larger than the integral length scale. Although the −1 power law scaling is often observed in neutral conditions for the streamwise velocity spectrum (Calaf et al., 2013; Drobinski et al., 2004; Katul et al., 1995, 1996, 2012; Marusic & Monty, 2019), previous studies also showed that such a −1 power law scaling ceases to exist under moderately stable stratification (Krug et al., 2019). To support this argument, the streamwise and vertical velocity spectra are computed from the CASES-99 data and are shown in Figure S2 in Supporting Information S1. Clearly, the low frequency components of both streamwise and vertical velocity spectra are closer to a zero power law scaling than a −1 power law scaling. Therefore, the streamwise and vertical velocity spectra are described as

$$E_u(k) = \begin{cases} C_u \epsilon^{\frac{2}{3}} L_h^{\frac{5}{3}}, & \text{if } k \le \frac{1}{L_h} \\ C_u \epsilon^{\frac{2}{3}} k^{-\frac{5}{3}}, & \text{if } k > \frac{1}{L_h} \end{cases} \tag{3}$$

$$E_w(k) = \begin{cases} C_w \epsilon^{\frac{2}{3}} L_v^{\frac{5}{3}}, & \text{if } k \le \frac{1}{L_v} \\ C_w \epsilon^{\frac{2}{3}} k^{-\frac{5}{3}}, & \text{if } k > \frac{1}{L_v} \end{cases} \tag{4}$$

where $E_u(k)$ and $E_w(k)$ denote the streamwise and vertical velocity spectrum respectively, $C_u = \frac{18}{55} \times 1.5$ and $C_w = \frac{24}{55} \times 1.5$ are the Kolmogorov spectral constants for one-dimensional velocity spectrum, and k denotes the one-dimensional wavenumber. Integrating Equations 3 and 4 within $0 < k < \infty$ yield

$$\sigma_u^2 = 2.5 C_u \epsilon^{\frac{2}{3}} L_h^{\frac{2}{3}}, \tag{5}$$

$$\sigma_w^2 = 2.5 C_w \epsilon^{\frac{2}{3}} L_v^{\frac{2}{3}}. \tag{6}$$

Invoking the definitions for F_h and F_v gives

$$\left(\frac{F_h}{F_v}\right)^{\frac{2}{3}} = \frac{C_u}{C_w} \frac{\sigma_w^2}{\sigma_u^2}. \tag{7}$$

To close Equation 7, we need to further examine the relation between σ_u^2 and σ_w^2.

It was suggested that turbulence kinetic energy (TKE) and σ_u^2 is at a balance as TKE $= \frac{1}{2}\left(\sigma_u^2 + \sigma_v^2 + \sigma_w^2\right) \approx \sigma_u^2$ (Banerjee et al., 2016) when turbulence is separated from gravity waves. Namely,

$$\sigma_u^2 \approx \sigma_v^2 + \sigma_w^2, \tag{8}$$

where σ_v indicates the standard deviation of velocity in the spanwise direction. The 1:1 comparison between σ_u^2 and $\sigma_v^2 + \sigma_w^2$ is shown in Figure S3 in Supporting Information S1 to support Equation 8. The standard deviation of spanwise velocity in Equation 8 can be closed by the spanwise velocity variance budget for stationary and horizontally homogeneous surface layer flows which reads

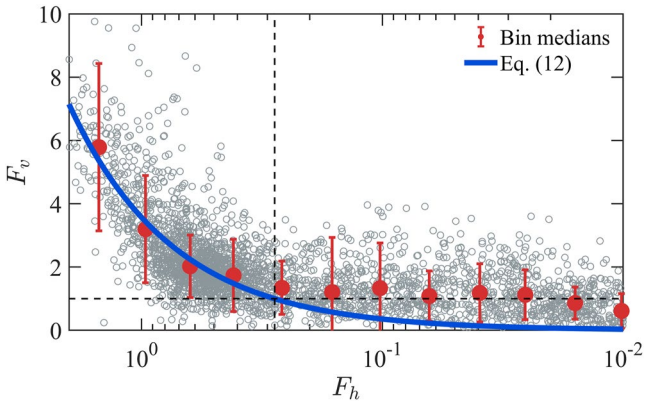

Figure 1. The relation between vertical Froude number F_v and horizontal Froude number F_h. The red dots and vertical bars refer to the median values and corresponding standard deviations in F_h bins, respectively. Each bin has a logarithmically equal width of 0.2. The blue solid line denotes Equation 12. The horizontal and vertical black dashed lines indicate the unit F_v and the critical horizontal Froude number $F_{hc} = 0.28$, respectively. Note that x-axis is reversed so that moving toward the right of this figure indicates an increase in the stable stratification.

$$\epsilon_v = \overline{\frac{P'}{\rho}\left(\frac{\partial v'}{\partial y}\right)}, \tag{9}$$

where ϵ_v denotes the TKE dissipation rate in the spanwise direction, P denotes the pressure, and ρ denotes the air density. Vertical transport term is neglected because the magnitude of this term is small compared with other terms under mild to moderate stratification (e.g., Li et al., 2016). The term on the left-hand side of Equation 9 can be estimated as $\frac{1}{3}\epsilon$ because small-scale energy dissipation is isotropic (Lindborg, 2006). The term on the right-hand side of Equation 9 is the correlation between pressure fluctuations and velocity shears that describe how TKE is redistributed by pressure perturbations. Traditionally, Rotta's return-to-isotropy hypothesis (Rotta, 1951) is used to parameterize this pressure correlation term in atmospheric boundary layer modeling (e.g., Katul et al., 2014; Zilitinkevich et al., 2007), which is expressed as (Pope, 2000):

$$2\overline{\frac{P'}{\rho}\left(\frac{\partial v'}{\partial y}\right)} = -\frac{C_r}{\tau}\left(\sigma_v^2 - \frac{2}{3}\mathrm{TKE}\right), \tag{10}$$

where $C_r = 1.8$ is the Rotta constant and τ is a relaxation time scale representing how fast TKE is dissipated. Here we formulate $\tau = \frac{\sigma_v^2}{2\epsilon_v}$ to focus on the spanwise TKE content relative to its dissipation rate. Equations 9 and 10 give the form of σ_v^2 as:

$$\sigma_v^2 = \frac{2}{3}\frac{C_r}{C_r + 1}\sigma_u^2. \tag{11}$$

Then, by substituting Equations 8 and 11 into Equation 7, the sought relation can be derived:

$$F_h = F_v\left(\frac{C_u}{C_w}\frac{C_r + 3}{3C_r + 3}\right)^{\frac{3}{2}}. \tag{12}$$

At the transition, $F_{vc} = 1$, corresponding to a critical horizontal Froude number

$$F_{hc} = 0.28. \tag{13}$$

4. Results

Using the CASES-99 data, F_v is shown as a function of F_h in Figure 1. As one can see, Equation 12 is in good agreement with observations in weak stratification, supporting our theory. Note that a decrease in F_h, which corresponds to moving toward the right of Figure 1, indicates an increase in the stable stratification. When $F_h < F_{hc}$, the calculated F_v from Equation 12 deviates from the observed F_v, which remains around unit. This is consistent with the key assumption invoked in our model, namely, the transition concurs with the development of pancake vortices in the stable atmospheric boundary layers. The mean deviation of the observed F_v when $F_h > F_{hc}$ is 0.35, implying that the uncertainties introduced by calculation of the potential temperature gradient and estimation of the L_v have a relatively small impact on the results. To exclude the potential impact of self-correlation on Figure 1, the relations between L_v, L_b, and L_h are shown in Figure S4 in Supporting Information S1. It can be seen that when $F_h > F_{hc}$, the relationship between L_v and L_h is reasonably described by Equation 12. When $F_h < F_{hc}$, L_v is no longer correlated with L_h and instead becomes equal to L_b. In short, the observation evidence supports the use of a critical horizontal Froude number $F_{hc} = 0.28$ to indicate the development of pancake vortices in stable atmospheric boundary layers.

Following Sun et al. (2016), the HOST patterns are shown in Figure 2a. The magnitude of u_* is around 0.15 m s^{-1} or less in the weak turbulence regime and is above 0.15 m s^{-1} in the moderate turbulence regime. In this plot, the mean wind speed threshold used to separate the two turbulence regimes is height dependent. It is also site dependent as shown in other work (Mahrt et al., 2015; Van de Wiel et al., 2012). In contrast, when the u_* is plotted against F_h in Figure 2b, the critical horizontal Froude number $F_{hc} = 0.28$ well separates the two turbulence regimes. More

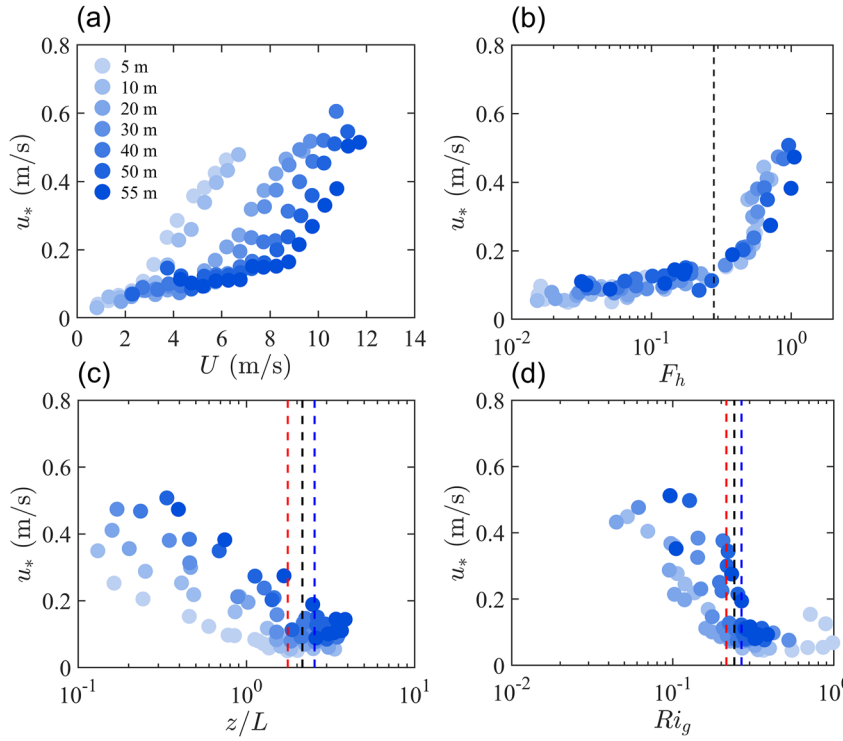

Figure 2. Relations between the friction velocity u_* and (a) the mean wind speed U, (b) the horizontal Froude number F_h, (c) z/L, and (d) the gradient Richardson number Ri_g. Data points are medians in mean wind speed bins, which are the same as those shown in (a). The black dashed lines indicate critical values of (b) F_h, (c) z/L, and (d) Ri_g. Blue and red dashed lines in (c, d) indicate the upper and lower limits of the critical values at the 95% confidence, respectively.

importantly, no height dependence is found. In this sense, F_{hc} is a better, non-dimensional threshold separating the two turbulent regimes.

One might be tempted to characterize the transition using traditionally defined stability parameters such as z/L and Ri_g. In the context of HOST patterns, Figures 2c and 2d shows that neither z/L nor Ri_g is a good indicator given the large scatter. However, it is insightful to estimate the critical values of z/L and Ri_g corresponding to F_{hc} as z/L and Ri_g are widely utilized in operational stable boundary layer parameterizations. To do so, all z/L and Ri_g data points in the interval $0.26 < F_h < 0.3$ are considered, which give a mean value of 2.15 ± 0.39 for z/L ($\pm$ refers to the 95% confidence interval) and a mean value of 0.241 ± 0.026 for Ri_g. Note that we do not observe strong variations of these values using other F_h intervals such as 0.27–0.29 or 0.25–0.31. These values, shown in Figures 2c and 2d, are consistent with those used in the literature (Galperin et al., 2007; Grachev et al., 2013; Li et al., 2015; Mahrt et al., 1998; Miles, 1961; Sorbjan, 2010; Stull, 1988; Sun et al., 2016).

Our results may shed some insights into the meaning of critical Richardson numbers often quoted in the literature. Miles (1961) reported that wave-like perturbations are dynamically stable when the flow is characterized by a linearized Euler equation and when Ri_g exceeds some critical value. While this seemingly suggests that stable boundary layer flows would laminarize when Ri_g exceeds some critical value, this association of critical Ri_g with flow laminarization has been questioned (Galperin et al., 2007; Katul et al., 2014; Li et al., 2015; Zilitinkevich et al., 2007, 2013), namely, a critical Ri_g associated with flow laminarization is not supported by observational and modeling evidence. Nonetheless, many studies did report a maximum (sometimes also called critical but is called maximum in our study to avoid confusion) flux Richardson number (Ri_f) that indicates substantial changes in flow behaviors. When the atmospheric stability is weak (e.g., when the Ri_g is small), Ri_f increases nearly linearly with Ri_g. As the atmospheric stability becomes stronger, especially when the Ri_g exceeds a value of about 0.2–0.25 (consistent with the values shown in Figure 2b), the Ri_f no longer increases (or a maximum value for Ri_f is attained). Previous studies have provided important theoretical insights into the meaning of this maximum Ri_f. Using a reduced model based on the return to isotropy concept, Bou-Zeid et al. (2018) showed that the maximum Ri_f is reached with zero vertical turbulent fluctuations ($\sigma_w = 0$). Differently, Katul et al. (2014) and follow-up

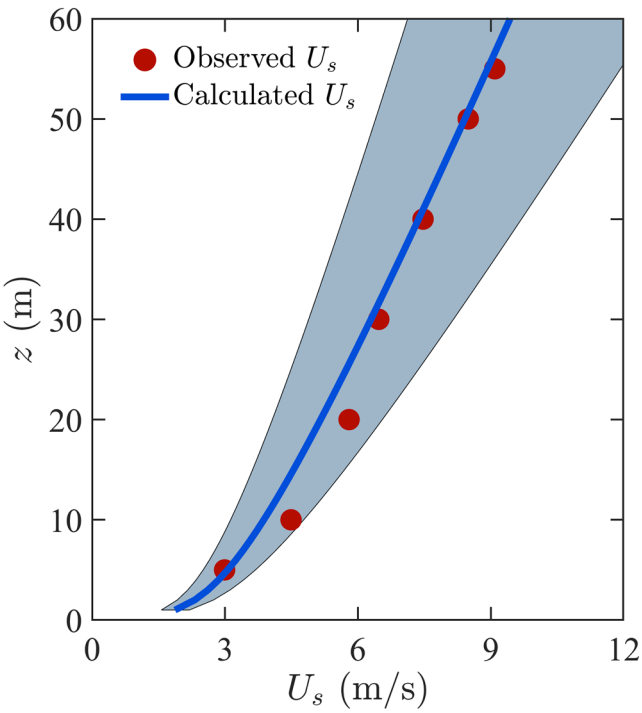

Figure 3. The vertical profiles of calculated U_s (blue line) by Equation 14. The red dots indicate observed U_s in Sun et al. (2012). The shading indicates 95% confidence intervals for the calculated U_s.

studies by Li et al. (2015) and Li (2019) interpreted the maximum Ri_f as the threshold beyond which the Kolmogorov scaling is no longer a distinct feature for turbulent velocity and temperature spectra, which is consistent with observational data presented in Grachev et al. (2013).

In this regard, our results have three important implications. First, our results imply that the turbulent flow in stable boundary layers does not become laminar under strong stratification when Ri_g exceeds 0.2–0.25 (see Figure 2d). Instead, the flow transitions to a weak turbulence regime characterized by pancake vortices, which provide a finite amount of turbulent mixing. Second, our model differs from that of Bou-Zeid et al. (2018) in that our model considers the structural characteristics of turbulence eddies and the transition identified by our model does not correspond to zero vertical turbulent fluctuations (i.e., two-dimensional turbulence). Previous studies have demonstrated that stably stratified turbulence still has a forward energy cascade, rather than an inverse energy cascade (Gucci et al., 2023; Sozza et al., 2015). Thus, it is important to recognize that although pancake vortices "look like" two dimensional, their dynamics remain three dimensional. Third, our model shares similarity with that of Katul et al. (2014) in that the spectra of horizontal and vertical velocity follow the Kolmogorov scaling at high wavenumber (Equations 3 and 4). The fact that our model results deviate from observational data when $F_h < F_{hc}$ (Figure 1) suggests that $F_h = F_{hc}$ is the point beyond which some key assumptions of our model break down. For example, velocity spectra in buoyancy subrange may differ from those described by Equations 3 and 4 when $F_h < F_{hc}$, as Kelvin–Helmholtz instabilities generated within pancake layers (Deloncle et al., 2008) can lead to the emergence of internal gravity waves. In this sense, F_{hc} has similarities with the maximum Ri_f suggested by Katul et al. (2014). However, we should emphasize that our model is formulated based on the horizontal Froude number while the model of Katul et al. (2014) yields an outcome regarding the flux Richardson number. Future work examining the connection between the critical horizontal Froude number, the maximum flux Richardson number, and internal gravity waves is welcome.

Lastly, we demonstrate that the mean wind speed threshold proposed by Sun et al. (2012) can be recovered from our theory. To do so we employ the stability-corrected logarithmic wind profile, which reads

$$U_s = \frac{u_{*s}}{\kappa}\left(\ln\left(\frac{z}{z_0}\right) + a_m\frac{z}{L_s}\right), \tag{14}$$

where the subscript s for u_* and L indicates the transition at $F_{hc} = 0.28$ (in practice the results at $F_{hc} = 0.28$ are approximately estimated by the averages over the range $0.26 < F_h < 0.3$ to reduce uncertainty), $a_m = 5$ is a constant, and z_0 is the roughness length which is taken to be 0.03 m following Van de Wiel et al. (2003). A comparison between the calculated U_s and the mean wind speed threshold identified by Sun et al. (2012) (denoted observed U_s) is shown in Figure 3, with an average difference of the two profiles less than 0.5 m s^{-1}. In Equation 14, we assume u_{*s} and L_s to be height-independent, although in reality, u_{*s} and L_s are slightly height-dependent, which may contribute to the slight underestimation of U_s below $z = 30$ m.

5. Conclusions and Discussion

The transition from moderate to weak turbulence regimes remains a challenge for stable boundary layer parameterizations in numerical weather and climate models. In this study, we propose a non-dimensional index for characterizing such transitions by invoking the development and evolution of pancake vortices. The length scale constraint of pancake vortices is introduced into a theoretical model, and the results show that a critical horizontal Froude number $F_{hc} = 0.28$ is capable to characterize the transition of turbulence regimes, which is supported by the CASES-99 data set. The critical values of z/L and Ri_g corresponding to F_{hc} are also estimated in this study; the mean values with 95% confidence intervals are 2.15 ± 0.39 for z/L and 0.241 ± 0.026 for Ri_g, respectively. While a z-dependent mean wind speed threshold was utilized to identify the transition in previous studies (Sun

et al., 2012), we find that the mean wind speed threshold can be recovered from F_{hc} through the stability-corrected logarithmic wind profile.

The findings in this study have broad implications. For instance, Sandu et al. (2013) reported that the representation of stably stratified turbulence in numerical weather prediction models remains a challenge, especially for the weak turbulence regime. Ren et al. (2022) documented that the rapid accumulation of pollutants is related to weak turbulence during heavy haze. The knowledge of the transition of turbulence regimes can be directly used to constrain the validity range of Monin-Obukhov similarity theory in numerical simulations for weather and pollutants dispersion. Although numerical models do not directly provide values of L_h, L_h can be linked to σ_u and ϵ through Equation 5, which are available in some turbulence parameterizations (Zilitinkevich et al., 2007, 2013). But future work needs to address how pancake vortices affect turbulent mixing efficiency and how to parameterize such mixing processes in numerical models. How pancake vortices differ from two-dimensional turbulence also needs to be studied. Moreover, the applicability of F_{hc} over mountainous regions requires further investigations because large-scale internal gravity waves induced by topography can transfer energy to turbulence (Sun et al., 2015). This process can potentially disturb the slicing process by zigzag instability due to enhanced connection between adjacent layers.

Data Availability Statement

The CASES-99 data set used in this study for turbulence variable calculation can be downloaded at https://www.eol.ucar.edu/content/integrated-surface-flux-facility-during-cases99. The code for turbulence variables calculations in this study is available at https://github.com/ShaoXin123/SBL_TurbulenceTransition.

Acknowledgments
This study is supported by the National Natural Science Foundation of China (Grants 42275065 and 41975006) and key innovation team of China Meteorological Administration (No. CMA2022ZD09). DL acknowledges support from the US-National Science Foundation (NSF) under the Award number AGS-1853354. The authors thank Otávio Acevedo and two other reviewers whose comments led to significant improvment of the quality of this paper.

References

Acevedo, O. C., Mahrt, L., Puhales, F. S., Costa, F. D., Medeiros, L. E., & Degrazia, G. A. (2016). Contrasting structures between the decoupled and coupled states of the stable boundary layer. *Quarterly Journal of the Royal Meteorological Society*, *142*(695), 693–702. https://doi.org/10.1002/qj.2693

Acevedo, O. C., Maroneze, R., Costa, F. D., Puhales, F. S., Degrazia, G. A., Nogueira Martins, L. G., et al. (2019). The nocturnal boundary layer transition from weakly to very stable. Part I: Observations. *Quarterly Journal of the Royal Meteorological Society*, *145*(725), 3577–3592. https://doi.org/10.1002/qj.3642

Banerjee, T., Li, D., Juang, J.-Y., & Katul, G. (2016). A spectral budget model for the longitudinal turbulent velocity in the stable atmospheric surface layer. *Journal of the Atmospheric Sciences*, *73*(1), 145–166. https://doi.org/10.1175/jas-d-15-0066.1

Billant, P., & Chomaz, J.-M. (2000a). Experimental evidence for a new instability of a vertical columnar vortex pair in a strongly stratified fluid. *Journal of Fluid Mechanics*, *418*, 167–188. https://doi.org/10.1017/s0022112000001154

Billant, P., & Chomaz, J.-M. (2000b). Theoretical analysis of the zigzag instability of a vertical columnar vortex pair in a strongly stratified fluid. *Journal of Fluid Mechanics*, *419*, 29–63. https://doi.org/10.1017/s0022112000001166

Billant, P., & Chomaz, J.-M. (2000c). Three-dimensional stability of a vertical columnar vortex pair in a stratified fluid. *Journal of Fluid Mechanics*, *419*, 65–91. https://doi.org/10.1017/s0022112000001178

Billant, P., & Chomaz, J.-M. (2001). Self-similarity of strongly stratified inviscid flows. *Physics of Fluids*, *13*(6), 1645–1651. https://doi.org/10.1063/1.1369125

Bou-Zeid, E., Gao, X., Ansorge, C., & Katul, G. G. (2018). On the role of return to isotropy in wall-bounded turbulent flows with buoyancy. *Journal of Fluid Mechanics*, *856*, 61–78. https://doi.org/10.1017/jfm.2018.693

Calaf, M., Hultmark, M., Oldroyd, H. J., Simeonov, V., & Parlange, M. B. (2013). Coherent structures and the k−1 spectral behaviour. *Physics of Fluids*, *25*(12). https://doi.org/10.1063/1.4834436

Chechin, D. (2021). On the u⋆−U relationship in the stable atmospheric boundary layer over Arctic sea ice. *Atmosphere*, *12*(5), 591. https://doi.org/10.3390/atmos12050591

Cheng, Y., Li, Q., Argentini, S., Sayde, C., & Gentine, P. (2020). A model for turbulence spectra in the equilibrium range of the stable atmospheric boundary layer. *Journal of Geophysical Research: Atmospheres*, *125*(5). https://doi.org/10.1029/2019jd032191

Cuxart, J., Morales, G., Terradellas, E., & Yagüe, C. (2002). Study of coherent structures and estimation of the pressure transport terms for the nocturnal stable boundary layer. *Boundary-Layer Meteorology*, *105*(2), 305–328. https://doi.org/10.1023/a:1019974021434

Deloncle, A., Billant, P., & Chomaz, J.-M. (2008). Nonlinear evolution of the zigzag instability in stratified fluids: A shortcut on the route to dissipation. *Journal of Fluid Mechanics*, *599*, 229–239. https://doi.org/10.1017/s0022112007000109

Drobinski, P., Carlotti, P., Newsom, R. K., Banta, R. M., Foster, R. C., & Redelsperger, J.-L. (2004). The structure of the near-neutral atmospheric surface layer. *Journal of the Atmospheric Sciences*, *61*(6), 699–714. https://doi.org/10.1175/1520-0469(2004)061<0699:Tsotna>2.0.Co;2

Foken, T. (2006). 50 years of the Monin–Obukhov similarity theory. *Boundary-Layer Meteorology*, *119*(3), 431–447. https://doi.org/10.1007/s10546-006-9048-6

Galperin, B., Sukoriansky, S., & Anderson, P. S. (2007). On the critical Richardson number in stably stratified turbulence. *Atmospheric Science Letters*, *8*(3), 65–69. https://doi.org/10.1002/asl.153

Grachev, A. A., Andreas, E. L., Fairall, C. W., Guest, P. S., & Persson, P. O. G. (2013). The critical Richardson number and limits of applicability of local similarity theory in the stable boundary layer. *Boundary-Layer Meteorology*, *147*(1), 51–82. https://doi.org/10.1007/s10546-012-9771-0

Gucci, F., Giovannini, L., Stiperski, I., Zardi, D., & Vercauteren, N. (2023). Sources of anisotropy in the Reynolds stress tensor in the stable boundary layer. *Quarterly Journal of the Royal Meteorological Society*, *149*(750), 277–299. https://doi.org/10.1002/qj.4407

Herring, J. R., & Métais, O. (1989). Numerical experiments in forced stably stratified turbulence. *Journal of Fluid Mechanics*, *202*, 97–115. https://doi.org/10.1017/s0022112089001114

Holtslag, A. A. M., Svensson, G., Baas, P., Basu, S., Beare, B., Beljaars, A. C. M., et al. (2013). Stable atmospheric boundary layers and diurnal cycles: Challenges for weather and climate models. *Bulletin of the American Meteorological Society*, *94*(11), 1691–1706. https://doi.org/10.1175/bams-d-11-00187.1

Hong, S.-Y., Noh, Y., & Dudhia, J. (2006). A new vertical diffusion package with an explicit treatment of entrainment processes. *Monthly Weather Review*, *134*(9), 2318–2341. https://doi.org/10.1175/mwr3199.1

Howard, L. N. (1961). Note on a paper of John W. Miles. *Journal of Fluid Mechanics*, *10*(04), 509. https://doi.org/10.1017/s0022112061000317

Katul, G. G., Albertson, J. D., Parlange, M. B., Hsieh, C.-I., Conklin, P. S., Sigmon, J. T., & Knoerr, K. R. (1996). The "Inactive" Eddy motion and the large-scale turbulent pressure fluctuations in the dynamic sublayer. *Journal of the Atmospheric Sciences*, *53*(17), 2512–2524. https://doi.org/10.1175/1520-0469(1996)053<2512:Tematl>2.0.Co;2

Katul, G. G., Chu, C. R., Parlange, M. B., Albertson, J. D., & Ortenburger, T. A. (1995). Low-wavenumber spectral characteristics of velocity and temperature in the atmospheric surface layer. *Journal of Geophysical Research*, *100*(D7), 14243. https://doi.org/10.1029/94jd02616

Katul, G. G., Porporato, A., & Nikora, V. (2012). Existence of k(-)(1) power-law scaling in the equilibrium regions of wall-bounded turbulence explained by Heisenberg's eddy viscosity. *Physical Review E - Statistical, Nonlinear and Soft Matter Physics*, *86*(6 Pt 2), 066311. https://doi.org/10.1103/PhysRevE.86.066311

Katul, G. G., Porporato, A., Shah, S., & Bou-Zeid, E. (2014). Two phenomenological constants explain similarity laws in stably stratified turbulence. *Physical Review E*, *89*(2), 023007. https://doi.org/10.1103/PhysRevE.89.023007

Kolmogorov, A. N. (1941). The local structure of turbulence in incompressible viscous fluid for very large Reynolds numbers. *Doklady Akademii Nauk SSSR*, *30*, 299–303.

Krug, D., Baars, W. J., Hutchins, N., & Marusic, I. (2019). Vertical coherence of turbulence in the atmospheric surface layer: Connecting the hypotheses of Townsend and davenport. *Boundary-Layer Meteorology*, *172*(2), 199–214. https://doi.org/10.1007/s10546-019-00445-4

Lan, C., Liu, H., Katul, G. G., Li, D., & Finn, D. (2019). Large eddies regulate turbulent flux gradients in coupled stable boundary layers. *Geophysical Research Letters*, *46*(11), 6090–6100. https://doi.org/10.1029/2019gl082228

Lan, C., Liu, H., Li, D., Katul, G. G., & Finn, D. (2018). Distinct turbulence structures in stably stratified boundary layers with weak and strong surface shear. *Journal of Geophysical Research: Atmospheres*, *123*(15), 7839–7854. https://doi.org/10.1029/2018jd028628

Lapworth, A., & Osborne, S. R. (2020). The nocturnal wind speed and sensible heat flux over flat terrain. *Boundary-Layer Meteorology*, *176*(3), 401–413. https://doi.org/10.1007/s10546-020-00534-9

Leweke, T., & Williamson, C. H. K. (1998). Cooperative elliptic instability of a vortex pair. *Journal of Fluid Mechanics*, *360*, 85–119. https://doi.org/10.1017/s0022112097008331

Li, D. (2019). Turbulent Prandtl number in the atmospheric boundary layer - Where are we now? *Atmospheric Research*, *216*, 86–105. https://doi.org/10.1016/j.atmosres.2018.09.015

Li, D. (2020). The O'KEYPS equation AND 60 years beyond. *Boundary-Layer Meteorology*, *179*(1), 19–42. https://doi.org/10.1007/s10546-020-00585-y

Li, D., Katul, G. G., & Bou-Zeid, E. (2015). Turbulent energy spectra and cospectra of momentum and heat fluxes in the stable atmospheric surface layer. *Boundary-Layer Meteorology*, *157*(1), 1–21. https://doi.org/10.1007/s10546-015-0048-2

Li, D., Salesky, S. T., & Banerjee, T. (2016). Connections between the Ozmidov scale and mean velocity profile in stably stratified atmospheric surface layers. *Journal of Fluid Mechanics*, *797*, R3. https://doi.org/10.1017/jfm.2016.311

Lindborg, E. (2006). The energy cascade in a strongly stratified fluid. *Journal of Fluid Mechanics*, *550*(1), 207. https://doi.org/10.1017/s0022112005008128

Mahrt, L. (2014). Stably stratified atmospheric boundary layers. *Annual Review of Fluid Mechanics*, *46*(1), 23–45. https://doi.org/10.1146/annurev-fluid-010313-141354

Mahrt, L., Sun, J., Blumen, W., Delany, T., & Oncley, S. (1998). Nocturnal boundary-layer regimes. *Boundary-Layer Meteorology*, *88*(2), 255–278. https://doi.org/10.1023/a:1001171313493

Mahrt, L., Sun, J., & Stauffer, D. (2015). Dependence of turbulent velocities on wind speed and stratification. *Boundary-Layer Meteorology*, *155*(1), 55–71. https://doi.org/10.1007/s10546-014-9992-5

Malhi, Y. S. (1995). The significance of the dual solutions for heat fluxes measured by the temperature fluctuation method in stable conditions. *Boundary-Layer Meteorology*, *74*(4), 389–396. https://doi.org/10.1007/bf00712379

Maroneze, R., Acevedo, O. C., Costa, F. D., Puhales, F. S., Demarco, G., & Mortarini, L. (2019). The nocturnal boundary layer transition from weakly to very stable. Part II: Numerical simulation with a second-order model. *Quarterly Journal of the Royal Meteorological Society*, *145*(725), 3593–3608. https://doi.org/10.1002/qj.3643

Marusic, I., & Monty, J. P. (2019). Attached Eddy model of wall turbulence. *Annual Review of Fluid Mechanics*, *51*(1), 49–74. https://doi.org/10.1146/annurev-fluid-010518-040427

Mater, B. D., & Venayagamoorthy, S. K. (2014a). The quest for an unambiguous parameterization of mixing efficiency in stably stratified geophysical flows. *Geophysical Research Letters*, *41*(13), 4646–4653. https://doi.org/10.1002/2014gl060571

Mater, B. D., & Venayagamoorthy, S. K. (2014b). A unifying framework for parameterizing stably stratified shear-flow turbulence. *Physics of Fluids*, *26*(3). https://doi.org/10.1063/1.4868142

Miles, J. W. (1961). On the stability of heterogeneous shear flows. *Journal of Fluid Mechanics*, *10*(04), 496. https://doi.org/10.1017/s0022112061000305

Miles, J. W., & Howard, L. N. (1964). Note on a heterogeneous shear flow. *Journal of Fluid Mechanics*, *20*(2), 331–336. https://doi.org/10.1017/s0022112064001252

Monin, A. S., & Obukhov, A. M. (1954). *Basic laws of turbulent mixing in the atmosphere near the ground* (Vol. 24, pp. 163–187). Tr AkadNauk SSSR Geofiz Inst.

Mortarini, L., Cava, D., Giostra, U., Costa, F. D., Degrazia, G., Anfossi, D., & Acevedo, O. (2019). Horizontal meandering as a distinctive feature of the stable boundary layer. *Journal of the Atmospheric Sciences*, *76*(10), 3029–3046. https://doi.org/10.1175/jas-d-18-0280.1

Nakanishi, M., & Niino, H. (2006). An improved Mellor–Yamada level-3 model: Its numerical stability and application to a regional prediction of advection fog. *Boundary-Layer Meteorology*, *119*(2), 397–407. https://doi.org/10.1007/s10546-005-9030-8

Nieuwstadt, F. T. M. (1984). The turbulent structure of the stable, nocturnal boundary layer. *Journal of the Atmospheric Sciences*, *41*(14), 2202–2216. https://doi.org/10.1175/1520-0469(1984)041<2202:Ttsots>2.0.Co;2

Peltola, O., Lapo, K., & Thomas, C. K. (2021). A physics-based universal indicator for vertical decoupling and mixing across canopies architectures and dynamic stabilities. *Geophysical Research Letters*, *48*(5), e2020GL091615. https://doi.org/10.1029/2020gl091615

Pleim, J. E. (2007). A combined local and nonlocal closure model for the atmospheric boundary layer. Part I: Model description and testing. *Journal of Applied Meteorology and Climatology*, *46*(9), 1383–1395. https://doi.org/10.1175/jam2539.1

Pope, S. (2000). *Turbulent flows*. Cambridge University Press.

Poulos, G. S., Blumen, W., Fritts, D. C., Lundquist, J. K., Sun, J., Burns, S. P., et al. (2002). CASES-99: A comprehensive investigation of the stable nocturnal boundary layer. *Bulletin of the American Meteorological Society*, *83*(4), 555–581. https://doi.org/10.1175/1520-0477(2002)083<0555:Caciot>2.3.Co;2

Ren, Y., Zhang, H., Zhang, X., Wu, B., Cai, X., Song, Y., & Zhu, T. (2022). Quantitative verification of the turbulence barrier effect during heavy haze pollution events. *Environmental Research Communications*, *4*(4), 045005. https://doi.org/10.1088/2515-7620/ac6381

Riley, J. J., & Lindborg, E. (2008). Stratified turbulence: A possible interpretation of some geophysical turbulence measurements. *Journal of the Atmospheric Sciences*, *65*(7), 2416–2424. https://doi.org/10.1175/2007jas2455.1

Rotta, J. (1951). Statistische Theorie Nichthomogener Turbulenz. *Zeitschrift fr Physik*, *129*(6), 547–572. https://doi.org/10.1007/bf01330059

Salesky, S. T., Katul, G. G., & Chamecki, M. (2013). Buoyancy effects on the integral lengthscales and mean velocity profile in atmospheric surface layer flows. *Physics of Fluids*, *25*(10). https://doi.org/10.1063/1.4823747

Sandu, I., Beljaars, A., Bechtold, P., Mauritsen, T., & Balsamo, G. (2013). Why is it so difficult to represent stably stratified conditions in numerical weather prediction (NWP) models? *Journal of Advances in Modeling Earth Systems*, *5*(2), 117–133. https://doi.org/10.1002/jame.20013

Sorbjan, Z. (2010). Gradient-based scales and similarity laws in the stable boundary layer. *Quarterly Journal of the Royal Meteorological Society*, *136*(650), 1243–1254. https://doi.org/10.1002/qj.638

Sozza, A., Boffetta, G., Muratore-Ginanneschi, P., & Musacchio, S. (2015). Dimensional transition of energy cascades in stably stratified forced thin fluid layers. *Physics of Fluids*, *27*(3). https://doi.org/10.1063/1.4915074

Stull, R. B. (1988). *An introduction to boundary layer meteorology*. Kluwer Acad. Publ.

Sun, J., Lenschow, D. H., LeMone, M. A., & Mahrt, L. (2016). The role of Large-Coherent-Eddy transport in the atmospheric surface layer based on CASES-99 observations. *Boundary-Layer Meteorology*, *160*(1), 83–111. https://doi.org/10.1007/s10546-016-0134-0

Sun, J., Mahrt, L., Banta, R. M., & Pichugina, Y. L. (2012). Turbulence regimes and turbulence intermittency in the stable boundary layer during CASES-99. *Journal of the Atmospheric Sciences*, *69*(1), 338–351. https://doi.org/10.1175/jas-d-11-082.1

Sun, J., Nappo, C. J., Mahrt, L., Belušić, D., Grisogono, B., Stauffer, D. R., et al. (2015). Review of wave-turbulence interactions in the stable atmospheric boundary layer. *Reviews of Geophysics*, *53*(3), 956–993. https://doi.org/10.1002/2015rg000487

Sun, J., Takle, E. S., & Acevedo, O. C. (2020). Understanding physical processes represented by the Monin–Obukhov bulk formula for momentum transfer. *Boundary-Layer Meteorology*, *177*(1), 69–95. https://doi.org/10.1007/s10546-020-00546-5

Van de Wiel, B. J. H., Moene, A. F., Hartogensis, O. K., De Bruin, H. A. R., & Holtslag, A. A. M. (2003). Intermittent turbulence in the stable boundary layer over land. Part III: A classification for observations during CASES-99. *Journal of the Atmospheric Sciences*, *60*(20), 2509–2522. https://doi.org/10.1175/1520-0469(2003)060<2509:Ititsb>2.0.Co;2

Van de Wiel, B. J. H., Moene, A. F., Jonker, H. J. J., Baas, P., Basu, S., Donda, J. M. M., et al. (2012). The minimum wind speed for sustainable turbulence in the nocturnal boundary layer. *Journal of the Atmospheric Sciences*, *69*(11), 3116–3127. https://doi.org/10.1175/jas-d-12-0107.1

Zilitinkevich, S. S., Elperin, T., Kleeorin, N., & Rogachevskii, I. (2007). Energy- and flux-budget (EFB) turbulence closure model for stably stratified flows. Part I: Steady-state, homogeneous regimes. *Boundary-Layer Meteorology*, *125*(2), 167–191. https://doi.org/10.1007/s10546-007-9189-2

Zilitinkevich, S. S., Elperin, T., Kleeorin, N., Rogachevskii, I., & Esau, I. (2013). A hierarchy of energy- and flux-budget (EFB) turbulence closure models for stably-stratified geophysical flows. *Boundary-Layer Meteorology*, *146*(3), 341–373. https://doi.org/10.1007/s10546-012-9768-8